Progress In Electromagnetics Research C, Vol. 89, 27–38, 2019

A Study of Hybrid Wide Slot Antenna with Hybrid Parasitic Element for Wideband Applications

Barun Kumar, Bhupendra K. Shukla*, Ajay Somkuwar, and Deepak K. Raghuvanshi

Abstract—In this communication, a hybrid shaped wide slot antenna with hybrid parasitic element has been investigated which is fabricated on an FR-4 substrate ($\tan(\delta) = 0.02$, $\varepsilon_r = 4.3$). The mutual coupling (between the slot and tuning stub), tuning of resonating modes and bandwidth of the antenna are adjusted by changing the dimension of parasitic element and tuning stub. The measured fractional bandwidth of the proposed antenna is 146.82% for $S_{11} < -10$ dB which covers the frequency span from 0.92 to 6 GHz. This antenna exhibits resonances at 1.094, 1.56, 2.073, 2.67 and 4.02 GHz. Surface current distribution has been investigated, and series of equations are deduced for resonating frequencies. Radiation characteristic exhibits an eight-shaped pattern at fundamental mode frequency whereas at frequencies 2.85 and 3.91 GHz a distorted pattern has been observed. For understanding the behavior of the antenna, structural parameters are varied in specific ranges.

1. INTRODUCTION

In a wide slot antenna, the role of a parasitic element is very prominent because it enhances the mutual coupling between the slot and tuning element, impedance bandwidth, overlapping of modes and can also generate new resonating modes [1–3]. Modern communication system requires such antennas which have high impedance bandwidth, small size, high gain, and unidirectional or bidirectional radiation pattern. A wide slot antenna is a potential candidate which meets the above requirements. In addition, these antennas offer some other merits such as low profile, low cost, planar geometry, light weight, easy integration with microwave circuits and easy fabrication [4, 5]. The slot can be truncated on patch and ground plane which relocate the position of the resonating modes. Basically, slot changes the phase velocity ($v_p = 1/\sqrt{LC}$) of the modes (TM_{10}, TM_{01}, TM_{12} and TM_{20}), and it also changes the values of inductance (L) and capacitance (C) [6, 7]. The shape and location of the slot, parasitic element, and tuning elements decide the fractional bandwidth, tuning of resonating frequency and overlapping of resonating modes. In last two decades, various wide slot antennas have been reported. Some of the reported slot shapes are rectangular slot [8], P-shaped slot [9], fractal slot [10], pentagonal slot [11], elliptical slot [12], stepped-circular slot [13], tapered slot [14], and rotated slot [15]. A parasitic element is used in a wide slot antenna when the area of the slot is comparable with the area of the ground plane [16]. Jan and Wang reported a rhombus slot antenna with parasitic strips [3] and achieved the bandwidth of 108% from 1.8 GHz to 6.04 GHz. Moreover, the bandwidth of the antenna is changed by the rotation of the parasitic element. The reported pentagon slot antenna with the parasitic element covers the bandwidth from 3.281 GHz to 7.45 GHz [2]. In this communication, we present a hybrid shaped wide slot antenna with a hybrid parasitic element for wide band applications (GSM 1800, WiMAX, PCS and ITM-2000). This antenna covers the frequency span from 0.92 GHz to 6 GHz and exhibits the fractional bandwidth of 146.82% for $S_{11} < -10$ dB. Wideband operation is achieved by adjusting the radius of tuning stub, wide slot and the parasitic element. To understand the electromagnetic behavior of the antenna, current distribution and far-field characteristic at resonating frequencies 0.99, 1.48, 2.13, 2.85 and 3.91 GHz have been investigated.

Received 24 September 2018, Accepted 28 November 2018, Scheduled 13 December 2018
* Corresponding author: Bhupendra Kumar Shukla (bhupendrashuklaphd@gmail.com).
The authors are with the Maulana Azad National Institute of Technology, Bhopal, India.

2. ANTENNA CONFIGURATION

The physical structure of hybrid shaped wide slot antenna with parasitic element is displayed in Figure 1, which is positioned on the XY-plane, and Z axis is normal to the radiating structure. Tuning element with parameters R_{t1} (radius of the major axis), R_{t2} (radius of the minor axis) and feed line ($M_1 \times M_2$) are modeled on the top surface of the substrate. The fractional bandwidth of the proposed topology depends on the shape of the tuning element. The electromagnetic energy is delivered to tuning stub through the feed line. The characteristic impedance Z_0 of the feed line is estimated by Equation (1) which depends on the width of the feed (M_2) and height of the substrate (h).

$$Z_0 = \frac{\eta}{2\pi\sqrt{\varepsilon}_{reff}} \ln\left\{\frac{8h}{M_2} + \frac{0.25M_2}{h}\right\} \tag{1}$$

where η and ε_{reff} are intrinsic impedance of the free space and effective dielectric constant, respectively. The optimum dimensions with parameters are tabulated in Table 1. To produce large number of resonating modes, a composite wide slot which is the combination of elliptical, rectangular and trapezoidal slots has been created on bottom surface of the FR-4 substrate. To realize wide bandwidth, a hybrid parasitic element which is the union of elliptical and trapezoidal geometry is integrated on ground plane. Two triangular slots which are mirror images to each other are etched on bottom corners of the ground plane, which improves the fractional bandwidth of the antenna.

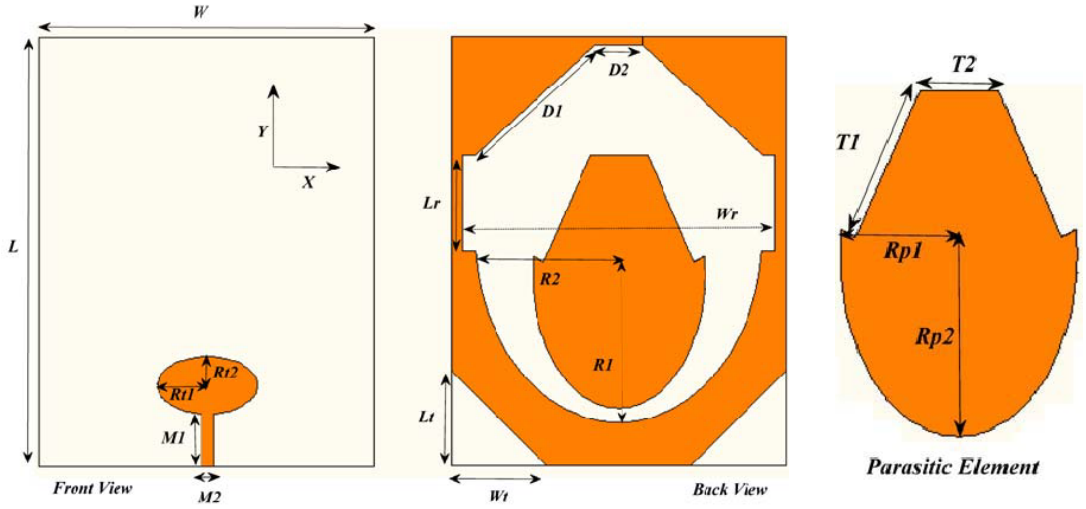

Figure 1. Geometry and parameters of hybrid shaped wide slot antenna.

3. DEVELOPMENT OF HYBRID WIDE SLOT ANTENNA

Figure 2 illustrates the progression of a composite wide slot antenna with a hybrid parasitic element. As shown in Figure 2 the geometry of the wide slot and parasitic element has been changed in consecutive steps whereas the shape of the tuning element remains constant. The frequency response of all antennas is shown in Figure 3. Antenna 1 ($A1$) comprises a regular shape wide slot and tuning element which has exhibited the fractional bandwidth ($BW(\%) = 200 * (f_h - f_l)/(f_h + f_l)$) of 69.66% from 2.9 to 6 GHz for $S_{11} < -10$ dB with two resonating frequencies at 4.51 and 5.73 GHz. Wide impedance bandwidth of the antenna depends on the superposition of resonating modes or generation of new resonance frequency near other resonating modes. In antenna 1, the area of the wide slot is comparable to the area of the ground plane. To achieve proper impedance matching in the entire frequency band (0.5 to 6 GHz), an elliptical shape parasitic element has been integrated on the ground plane, which retunes resonating frequencies. Antenna 2 ($A2$) shows dual-band frequency response (0.97 to 1.6 GHz with bandwidth 49.02% and 2.13 to 5.67 GHz with bandwidth 90.76%) with four resonating frequencies at 1.10, 2.41,

Table 1. Structural parameters and dimensions of hybrid shaped wide slot antenna.

Parameter	Dimension (mm)	Parameter	Dimension (mm)
M_1	11	R_1	39.5
M_2	2.6	R_2	30
L	90	R_{p1}	18
W	70	R_{p2}	28
R_{t1}	10.5	T_1	24.46
R_{t2}	6	T_2	12
L_r	20	D_1	33.97
W_r	65	D_2	10
L_t	20	W_t	20

3.37 and 5.34 GHz. In the next step ($A3$), the geometry of the elliptical shape wide slot has been amended which influences the position of higher and lower cutoff frequencies. In frequency band 0.97 to 1.6 GHz, the frequency separation between two resonating frequencies 1.09 and 1.21 GHz has been increased while in antenna 2 these frequencies are completely overlapped. Antenna 3 also exhibits dual-band frequency response with six resonating frequencies at 1.02, 1.21, 2.43, 3.55, 4.2 and 5.35 GHz.

For bandwidth augmentation, the shape of the wide slot is changed in antenna 4 ($A4$) which covers the frequency span from 0.905 to 5.58 GHz with fractional bandwidth 144.17%. Antenna 4 shows the resonance behavior at 0.96, 1.35, 2.19 and 5.03 GHz. The bandwidth of the antenna can be modified by changing the geometry of the parasitic element. In the next stage, the top of the parasitic element is amended by adding trapezoidal element. The positive impact of modification in parasitic element has been noticed in higher cutoff frequency. This antenna occupies the impedance bandwidth of 146.43% from 0.92 to 5.95 GHz with resonating frequencies 0.98, 1.44, 2.17, 3.76 and 5.26 GHz. In the final step, two symmetrical triangle-shaped slots are etched on the bottom edge of the ground plan which improves the higher cutoff frequency. The proposed antenna ($A6$) exhibits the fractional bandwidth of 146.82% from 0.92 to 6 GHz, and it also resonates at five frequencies 0.99, 1.48, 2.13, 2.85 and 3.91 GHz.

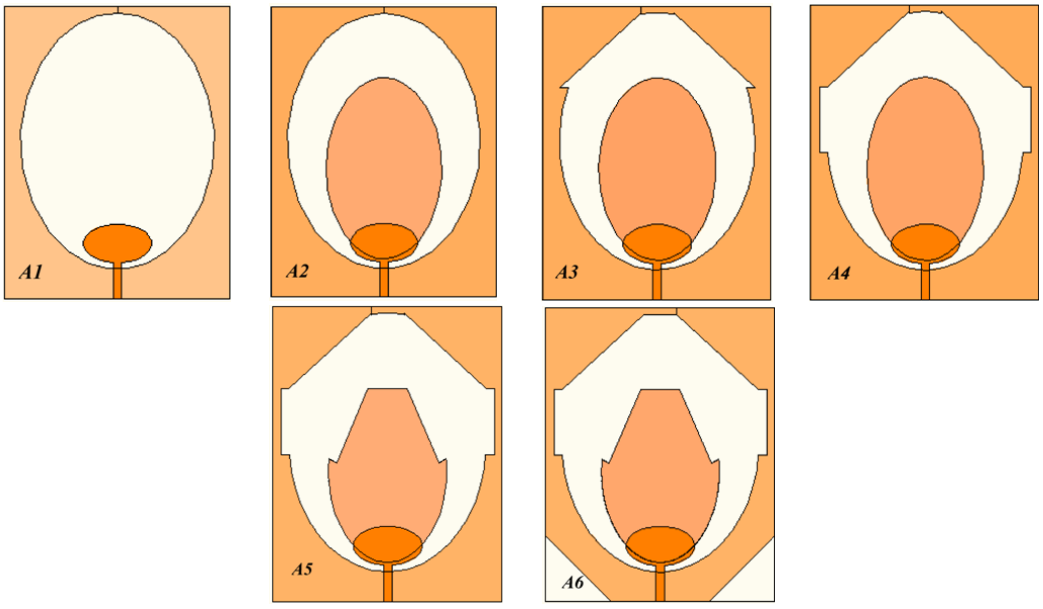

Figure 2. Development of hybrid shaped wide slot antenna with hybrid parasitic element.

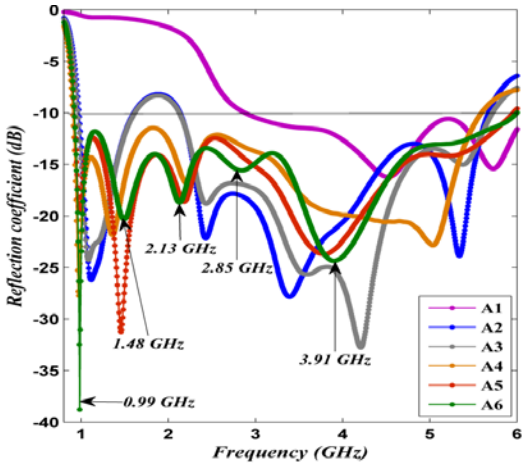

Figure 3. Reflection coefficient characteristics of antenna 1, 2, 3, 4 and 5.

4. STRUCTURAL PARAMETER ANALYSIS

For bandwidth optimization and to understand the electromagnetic behavior of the proposed antenna, the shape of the resonating elements has been varied by changing the dimension. In this study, only a single variable is varied at a time whereas other parameters are treated as constant.

4.1. Impact of Radius (R_1 and R_2) of Hybrid Shaped Wide Slot

Figure 4 displays the influence of R_1 and R_2 on reflection coefficient characteristic of the proposed antenna. It is investigated that by modifying R_1 (major axis radius of the wide slot), resonating frequencies (f_{r1}, f_{r2}, f_{r3}, f_{r4}, and f_{r5}) are developed, shifted and overlapped. Shifting of resonating frequencies is observed due to slow wave effect or tuning of effective capacitance. In addition, the impedance matching is improved in the entire frequency band due to the change in capacitive coupling between the parasitic patch and slot edge. Moreover, the higher cutoff frequency shifts downward. This happens because when R_1 is modified, the capacitance between a ground plane and tuning stub is also increased. It is observed that by increasing the R_2 (minor axis radius of the wide slot), the path length of current vectors has been increased which directly affects the position of the fundamental mode and lower cutoff frequency. The area of the slot also alters the inductance and capacitance of the

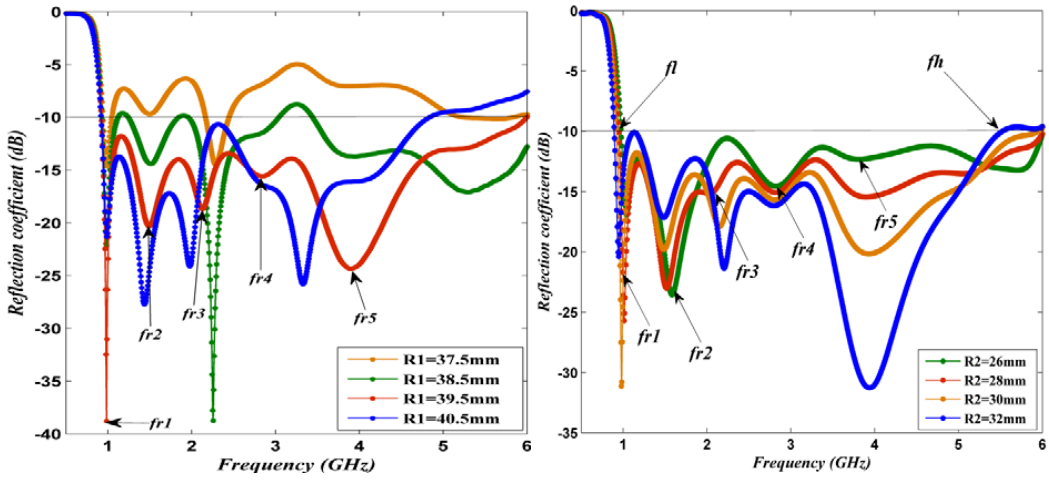

Figure 4. Impact of R_1 and R_2 on reflection coefficient characteristic of the proposed antenna.

antenna which changes the location of other resonance frequencies. The resonance frequencies f_{r1}, f_{r3} are shifted in downward direction whereas f_{r2} is shifted in upward direction. For a larger value of R_2, the impedance bandwidth of the antenna is deteriorated due to less mutual coupling between tuning stub and slot.

4.2. Impact of Radius (R_{p1} and R_{p2}) of Hybrid Shaped Parasitic Element

Figure 5 illustrates the impact of R_{p1} and R_{p2} on S_{11} characteristic of the proposed antenna. Modifying the parameter R_{p1} (minor axis radius of the parasitic element) from 16 mm to 20 mm, the matching level at f_{r1} and f_{r2} is improved whereas it decreases at f_{r3}. The higher cutoff frequency has shifted right, and bandwidth of the antenna is improved. This happens because the overlapping area of parasitic patch increases with tuning stub which improves the mutual coupling between slot and tuning stub. A larger value of R_{p1} critically affects the mid-frequency band and bandwidth of the antenna. This is because of over-coupling between slot edge and tuning element. With extension in R_{p2} (major axis radius of the parasitic element), the impedance matching at f_{r1}, f_{r2}, f_{r3}, f_{r4} and f_{r5} is modified. Furthermore, downshift of f_h (higher cutoff frequency) has been observed due to change in effective capacitance between the slot and parasitic element. The worst impedance bandwidth is investigated at $R_{p2} = 30$ mm. This occurs, due to over-coupling between the tuning element and parasitic element.

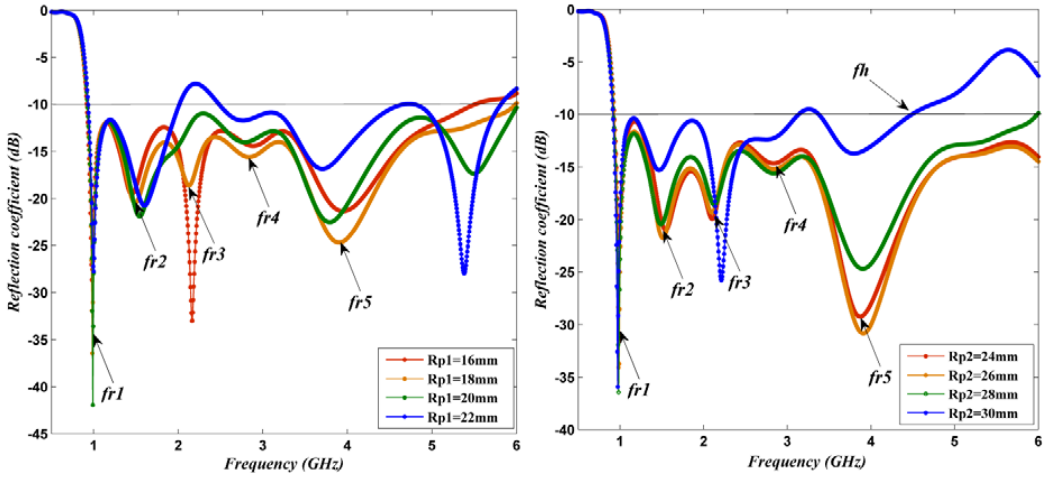

Figure 5. Impact of R_{p1} and R_{p2} on reflection coefficient characteristic of the proposed antenna.

4.3. Impact of Radius (R_{t1} and R_{t2}) of the Elliptical Shaped Tuning Stub

It is clear from Figure 6 that R_{t1} governs the impedance bandwidth, impedance matching and position of higher cutoff frequency. Modification of R_{t1} increases the overlapping area with the parasitic element. Due to this, the effective capacitance between the tuning stub and parasitic element has increased which decrease the higher cutoff frequency. The reduction in impedance bandwidth has been also observed. This occurs due to over coupling between the parasitic patch and tuning stub. The optimum bandwidth is found for $R_{t1} \leq 10.5$ mm. With the increase in R_{t2} (see Figure 6) from 4 mm to 7 mm, the impedance bandwidth is increased, and higher cutoff frequency is shifted towards the right. Due to modification in R_{t2}, the area of tuning stub increases, and the overlapping area between the tuning stub and parasitic patch is also increased. This increases the mutual coupling between elements (parasitic patch, slot and tuning stub). Modification of this parameter also increases the capacitance between parasitic element and tuning stub which upshifts the higher cutoff frequency. The higher value of $R_{t2} = 8$ mm disturbs the mid-frequency band and bandwidth of the antenna. This occurs due to over coupling between resonating elements.

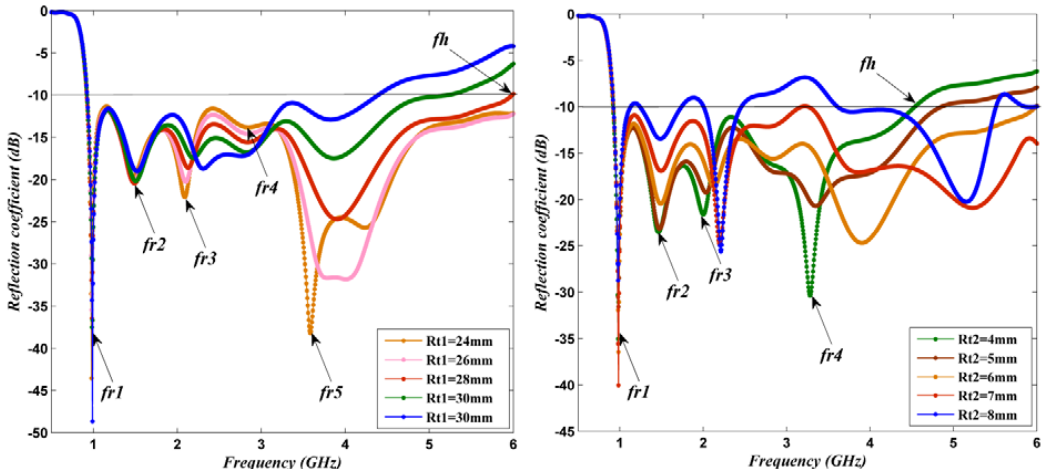

Figure 6. Impact of R_{t1} and R_{t2} on reflection coefficient characteristic of the proposed antenna.

5. RESULTS AND DISCUSSION

5.1. S_{11} Characteristic

The resonance behavior and impedance characteristics of this antenna are analyzed using CST Microwave Studio. After the numerical investigation, it is fabricated on an FR-4 substrate. A prototype of hybrid shaped wide slot antenna with the hybrid parasitic element is shown in Figure 7. We have designed hybrid slot and hybrid parasitic element because both elements offer flexibility to change in shape. By changing the shape, we can tune the location of resonating modes and achieve the overlapping of modes which is required for bandwidth enhancement. The experimental data are acquired from Agilent Technologies based Vector Network Analyzer N2223A in frequency span 0.8 to 6 GHz. After measurement, the experimentally and numerically analyzed reflection coefficient characteristics are compared, which is displayed in Figure 8. The measured fractional bandwidth of proposed antenna is 146.82% for $S_{11} < -10$ dB. The measured values of lower cutoff frequency (f_l) and higher cutoff frequency (f_h) are 0.92 and 6 GHz, respectively. This antenna exhibits resonances at 1.094, 1.56, 2.073, 2.67 and 4.02 GHz. Table 2 represents the error between simulated and measured lower cutoff frequencies and other resonating frequencies. Inconsistency is found between measured and simulated reflection coefficient characteristics and positions of resonance frequencies. This happens due to soldering loss, inhomogeneous permittivity, and fabrication error. Another cause of inconsistency considered is different dimensions of SMA connector during numerical analysis.

Figure 7. Prototype of hybrid shaped wide slot antenna.

Table 2. Error between measured and simulated resonating frequencies.

Frequency	Simulated (GHz)	Measured (GHz)	|Error (%)|
f_l	0.92	0.92	0
f_1	0.984	1.094	10.05
f_2	1.49	1.56	4.48
f_3	2.14	2.073	3.23
f_4	2.83	2.67	5.99
f_5	3.93	4.02	2.23

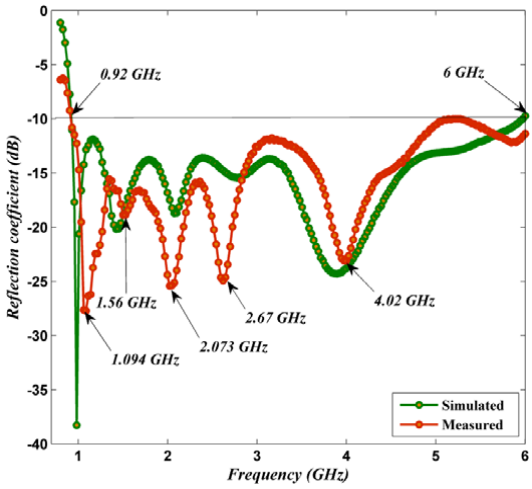

Figure 8. Comparison of simulated and measured reflection coefficient characteristic of the hybrid shape wide slot antenna with hybrid parasitic element.

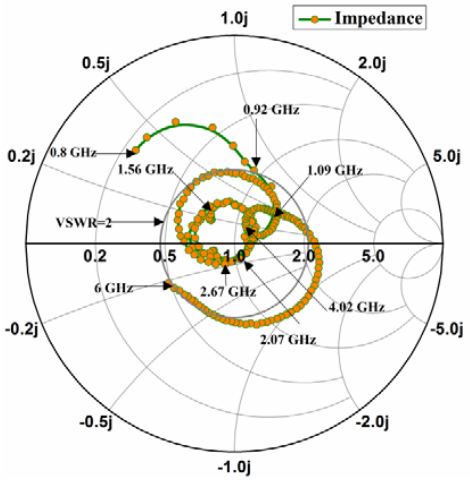

Figure 9. Measured input impedance of the hybrid shape wide slot antenna with hybrid parasitic element.

5.2. Input Impedance

The trace of the measured normalized input impedance of proposed antenna is depicted in Figure 9. Loops are formed in Smith chart due to overlapping of resonating modes or mutual coupling between modes. It is clear from the figure that wideband characteristic of the antenna is accomplished after overlapping of resonating frequencies 1.094, 1.56, 2.073, 2.67 and 4.02 GHz.

5.3. Current Distribution

At resonance frequencies, the vector current distribution of fabricated antenna is depicted in Figure 10. These current distributions are developed after the superposition of several resonating modes. The superposition of modes can be accomplished by changing the dimension of resonating elements like parasitic element, tuning stub and slot. As depicted in Figure 10, the number of half wave variations along the edges of the resonating elements is increased as operating frequency increases. After an investigation of surface current distribution, it has been found that the fundamental mode is developed due to the hybrid slot. At fundamental frequency (f_1) 0.99 GHz, the current vectors are scattered like TM_{10} mode on the parasitic element and tuning stub, and one half wave variation of current vectors is noticed along the boundary of the hybrid slot. It is distinguished that the current maximum occurs on the side edge of the ground plane and hybrid slot. This indicates that the antenna is operated by

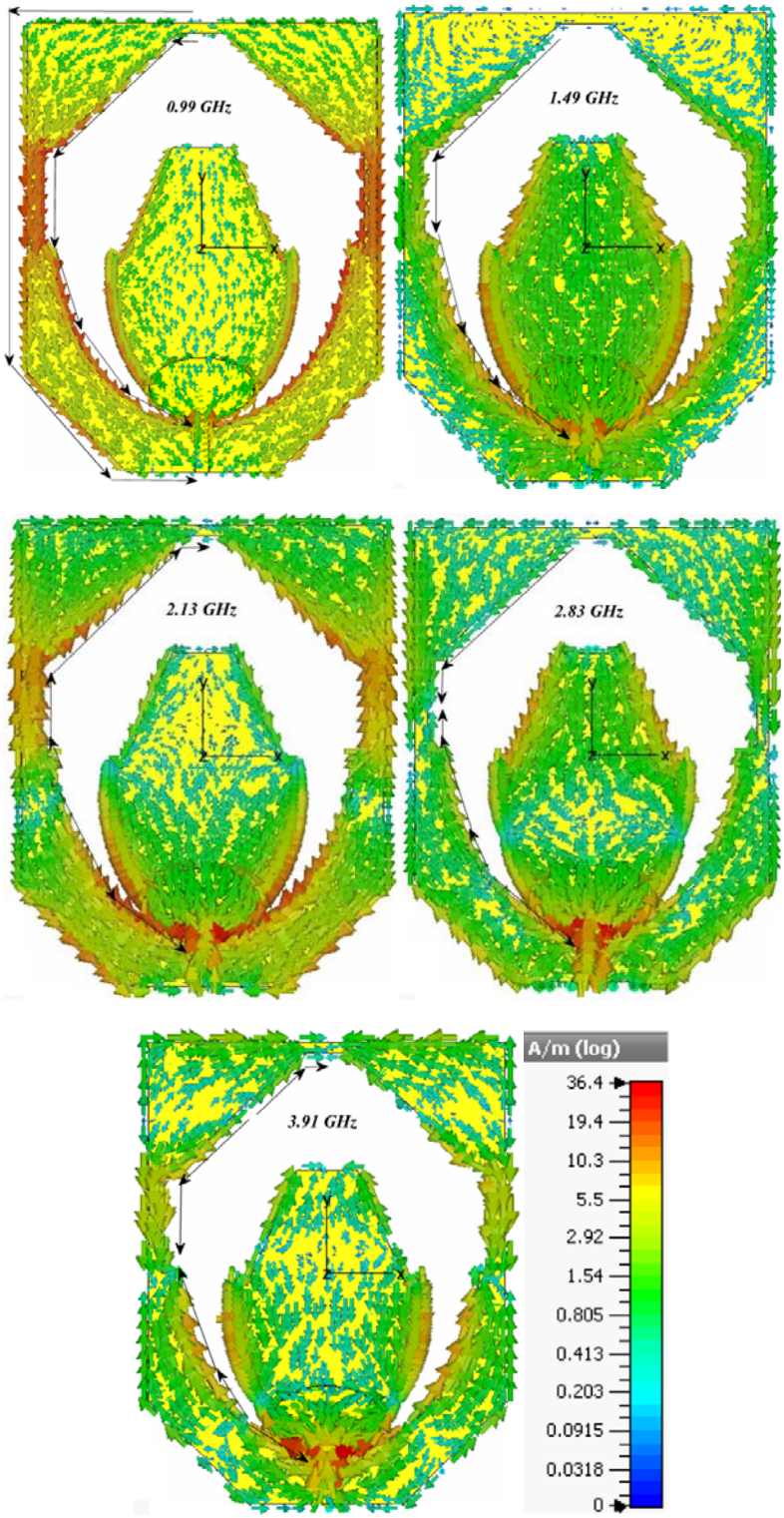

Figure 10. Simulated surface current distribution of proposed antenna at frequencies $f_1 = 0.99\,\text{GHz}$, $f_2 = 1.49\,\text{GHz}$, $f_3 = 2.13\,\text{GHz}$, $f_4 = 2.85\,\text{GHz}$ and $f_5 = 3.91\,\text{GHz}$.

fundamental mode which can be computed by following equations.

$$L_1 = D_2 + D_1 + L_r + (\pi/2) * \sqrt{(R_1^2 + R_2^2)/2} \tag{2}$$

$$f_1 = \frac{c}{L_1\sqrt{\varepsilon}_r} \tag{3}$$

where ε_r is the permittivity of the FR-4 substrate. The computed value of f_1 is 0.996 GHz which is nearly equal to the simulated value of f_1. The maximum size of the antenna decides the location of lower cutoff frequency of the antenna. For this antenna, f_l can be evaluated by the dimension of the side and top edges of the ground plane.

$$L_l = W + L - L_t - W_t + \sqrt{L_t^2 + W_t^2} \tag{4}$$

$$f_l = \frac{c}{L_l\sqrt{\varepsilon}_r} \tag{5}$$

The computed value of f_l is 0.93 GHz. An error of 1.075% is estimated between simulated (0.92 GHz) and computed lower cutoff frequencies. The fundamental mode of the parasitic element can be computed by below-given equations

$$L_{parasitic} = T_1 + \frac{T_2}{2} + 0.5 * \pi * \sqrt{(R_{p1}^2 + R_{p2}^2)/2} \tag{6}$$

$$f_{parasitic} = \frac{c}{L_{parasitic}\sqrt{\varepsilon}_r} \tag{7}$$

The computed value of $f_{parasitic}$ is 2.1 GHz. The broadband frequency response near 2.13 GHz is achieved after the overlapping of the second harmonic of the fundamental mode and fundamental mode of the parasitic element. At frequency 1.48 GHz, current is minimum at the top edge of the hybrid slot whereas like TM_{10} mode the current vectors are scattered on the parasitic element. Moreover, the strength of the current is higher on the bottom side of the hybrid slot, along the boundary of the parasitic element and bottom edge of the tuning element. The second resonating frequency can be calculated by equations below

$$L_2 = D_1 + L_r + (\pi/2) * \sqrt{(R_1^2 + R_2^2)/2} \tag{8}$$

$$f_2 = \frac{c}{L_2\sqrt{\varepsilon}_r} \tag{9}$$

The calculated value of f_2 is 1.3 GHz which is nearly equal to 1.48 GHz which is the simulated value of f_2. The estimated error between simulated and calculated f_2 is 12.58%. It is investigated that the harmonics of fundamental mode (f_1) and parasitic fundamental modes ($f_{parasitic}$) are also present in the reflection coefficient characteristic. It is noticed that the third resonating frequency ($f_3 = 2 * f_1$) is the second harmonics of the fundamental mode. At this frequency, two half wave variations of current vectors are perceived along the boundary of hybrid slot. The calculated and simulated values of f_3 are 1.99 and 2.13 GHz, respectively. The estimated error between simulated and calculated f_3 is 6.57%. The fourth resonating frequency ($f_4 = 3 * f_1$) is the third harmonics of the fundamental mode. At this frequency, three half wave variations of current vectors are perceived along the boundary of the hybrid slot. The calculated and simulated values of f_4 are 2.97 and 2.83 GHz, respectively. The estimated error between simulated and calculated f_4 is 4.71%. The fifth resonating frequency ($f_5 = 4 * f_1$) is the fourth harmonics of the fundamental mode. At this frequency, four half wave variations of current vectors are perceived along the boundary of the hybrid slot. The calculated and simulated values of f_5 are 3.96 and 3.93 GHz respectively. The estimated error between simulated and calculated f_5 is 0.75%. The second harmonic of parasitic fundamental mode ($f_0 = 2 * f_{parasitic}$) is 4.2 GHz which is situated near the fourth harmonics of the fundamental mode. The wideband frequency characteristic near 4 GHz band is accomplished after the overlapping of f_0 and f_5.

5.4. Radiation Pattern

Figure 11 illustrates the similarity between simulated and measured far-field patterns of hybrid slot antenna with the hybrid parasitic element. The radiation pattern is simulated and measured at frequencies 0.99, 1.48, 2.85 and 3.91 GHz. In E plane, the bidirectional pattern is measured at 0.99 GHz and 1.48 GHz whereas approximate eight-shape pattern is measured in the H plane at the

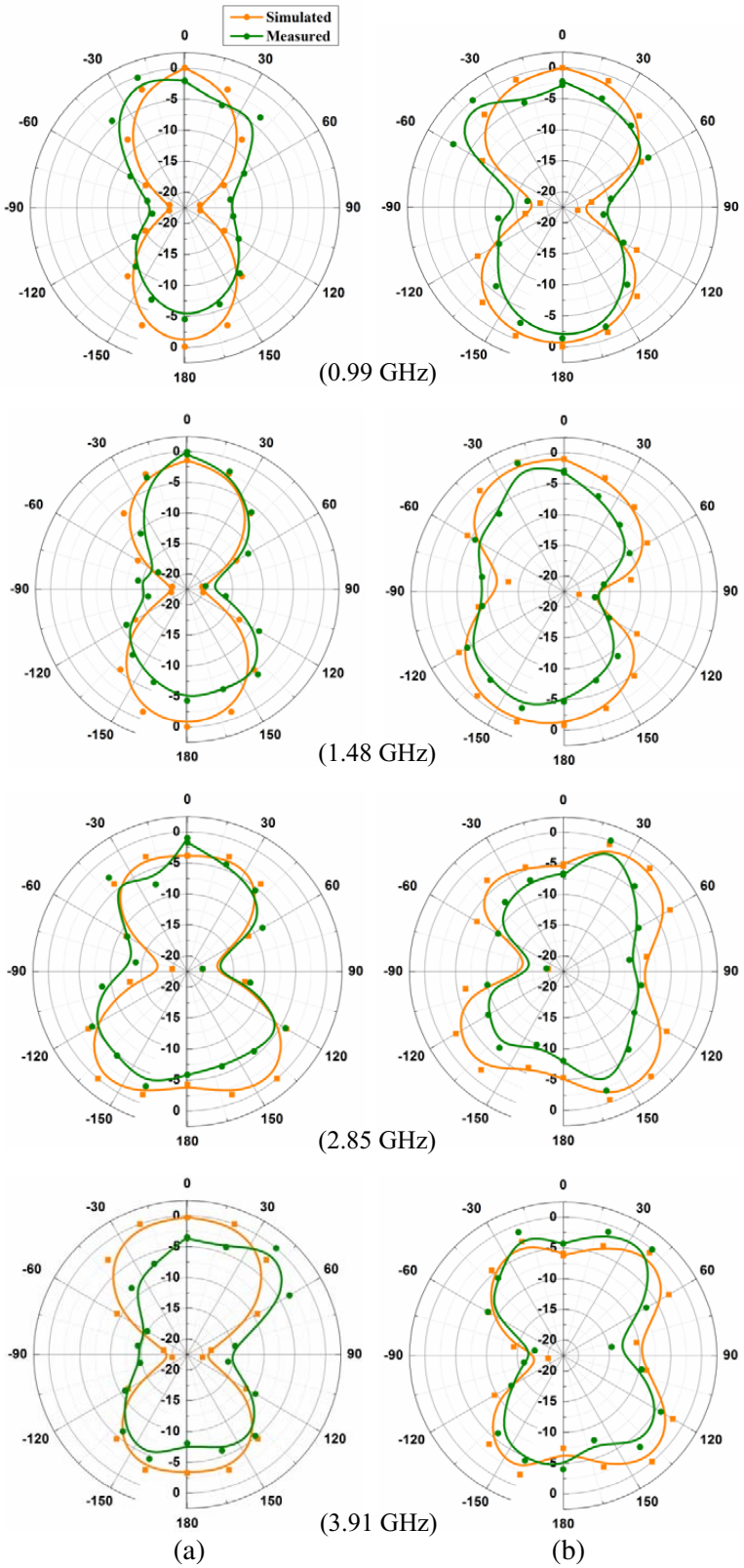

Figure 11. (a) E plane and (b) H plane pattern at frequencies $f_1 = 0.99\,\text{GHz}$, $f_2 = 1.48\,\text{GHz}$, $f_4 = 2.85\,\text{GHz}$ and $f_5 = 3.91\,\text{GHz}$.

same frequencies. In current distribution, it is investigated that multiple half wave variations of current vectors are found along the boundary of resonating elements and exhibit the existence of higher order modes. At frequencies 2.85 and 3.91 GHz, the shapes of the patterns in both planes are distorted. This occurs due to the existence of higher order modes. The inconsistency between measured and simulated far-field patterns is investigated due to fabrication error and radiation from the coaxial cable. The quantitative comparison of proposed antenna in terms of size and bandwidth with the existing antennas is shown in Table 3. All these antennas are designed on an FR-4 substrate. The proposed antenna exhibits a larger bandwidth. Figure 12 represents the gain and efficiency of the antenna. At higher frequency (6 GHz), the gain and efficiency of the antenna are dropped.

Table 3. Comparison of parameters of proposed antenna with existing antennas.

Reference	Size (mm × mm)	Lower cut off frequency	Higher cut off frequency	Bandwidth (%)	Slot shape	Parasitic shape
[2]	25 × 25	3.281 GHz	7.45 GHz	77.72	Pentagonal	Pentagonal
[3]	51.5 × 61	1.8 GHz	6.09 GHz	108	Rotated	Strip
[15]	70 × 70	3.4 GHz	5.6 GHz	49.4	Rotated	-
[16]	25 × 25	3.71 GHz	12.15 GHz	44.44, 67.03	Hexagonal	Hexagonal
[17]	37 × 37	2.23 GHz	5.35 GHz	80	Rotated	Square
Proposed	90 × 70	0.92 GHz	6 GHz	146.82	Composite	Hybrid

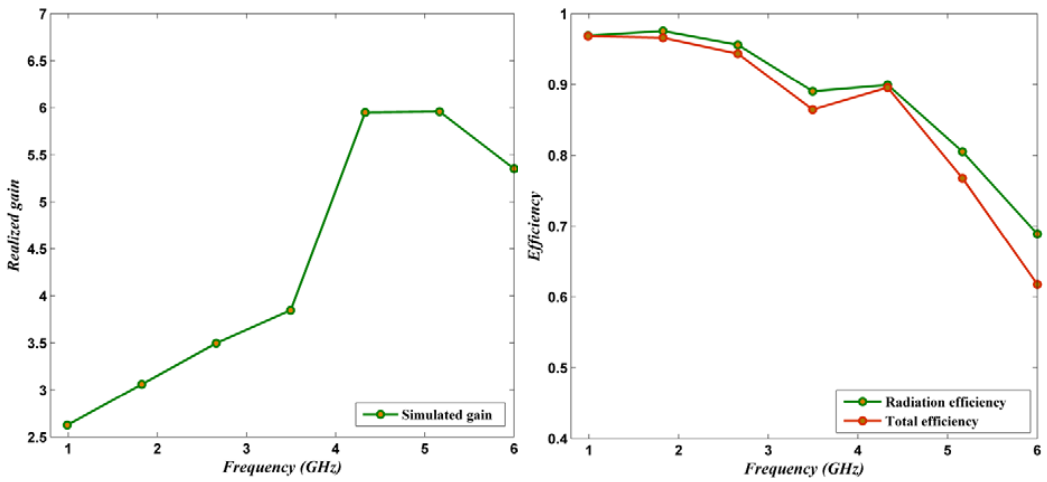

Figure 12. The simulated realized gain and efficiency of the proposed antenna.

6. CONCLUSION

A hybrid shaped wide slot antenna with a hybrid parasitic element has been fabricated and studied. It is noticed that mutual coupling (between slot and tuning stub), tuning of resonating modes and bandwidth of the antenna are adjusted by changing the dimension of parasitic element and tuning stub. This antenna offers the fractional bandwidth of 146.82% for $|S_{11}| < -10$ dB and covers the frequency range from 0.92 to 6 GHz. It exhibits resonances at 1.094, 1.56, 2.073, 2.67 and 4.02 GHz. For resonating frequencies, equations are developed after inspecting the surface current distribution. The far-field pattern is examined in E plane and H plane. The eight-shaped pattern is investigated at 0.99 GHz whereas at other frequencies distorted pattern is measured.

REFERENCES

1. Tang, M. C., R. W. Ziolkowski, and S. Xiao, "Compact hyper band printed slot antenna with stable radiation properties," *IEEE Transactions on Antennas and Propagation*, Vol. 62, No. 6, 2962–2969, June 2014.
2. Shinde, P. N. and J. P. Shinde, "Design of compact pentagonal slot antenna with bandwidth enhancement for multiband wireless applications," *AEU-International Journal of Electronics and Communications*, Vol. 69, 1489–1494, 2015.
3. Jan, J. Y. and L. C. Wang, "Printed wideband rhombus slot antenna with a pair of parasitic strips for multiband applications," *IEEE Transactions on Antennas and Propagation*, Vol. 57, 1267–1270, 2009.
4. Dastranj, A. and H. Abiri, "Bandwidth enhancement of printed E-shaped slot antennas fed by CPW and microstrip line," *IEEE Transactions on Antennas and Propagation*, Vol. 58, 1402–1407, 2010.
5. Zhong, Y. W., G. M. Yang, and L. R. Zheng, "Planar circular patch with elliptical slot antenna for ultra wideband communication applications," *Microwave and Optical Technology Letters*, Vol. 57, 325–328, 2015.
6. Al-Azza, A. A., F. J. Harackiewicz, and H. R. Gorla, "Very compact open-slot antenna for wireless communication systems," *Progress In Electromagnetics Research Letters*, Vol. 51, 73–78, 2015.
7. Deshmukh, A. A. and K. P. Ray, "Analysis of broadband variations of U-slot cut rectangular microstrip antennas," *IEEE Antennas and Propagation Magazine*, Vol. 57, 181–193, 2015.
8. Yao, F. W., S. S. Zhong, W. Wang, and X. L. Liang, "Wideband slot antenna with a novel microstrip feed," *Microwave and Optical Technology Letters*, Vol. 46, 275–278, 2005.
9. Tiang, S. S., M. F. Ain, and M. Z. Abdullah, "Compact and wideband wide-slot antenna for microwave imaging system," *IEEE International RF and Microwave Conference (RFM)*, 63–66, 2011.
10. Chen, W. L., G. M. Wang, and C. X. Zhang, "Bandwidth enhancement of a microstrip-line-fed printed wide-slot antenna with a fractal-shaped slot," *IEEE Transactions on Antennas and Propagation*, Vol. 57, 2176–2179, 2009.
11. Chen,, W. F., C. C. Tsai, and C. Y. Huang, "Compact wide-slot antenna for ultra-wideband communications," *Electronics Letters*, Vol. 44, 892–893, 2008.
12. Li, P., J. Liang, and X. Chen, "Study of printed elliptical/circular slot antennas for ultra wideband applications," *IEEE Transactions on antennas and Propagation*, Vol. 54, 1670–1675, 2006.
13. Abed, D., S. Redadaa, and H. Kimouche, "Printed ultra-wideband stepped-circular slot antenna with different tuning stubs," *Journal of Electromagnetic Waves and Applications*, Vol. 27, 846–855, 2013.
14. Azim, R., M. T. Islam, and N. Misran, "Compact tapered-shape slot antenna for UWB applications," *IEEE Antennas and Wireless Propagation Letters*, Vol. 10, 1190–1193, 2011.
15. Jan, J. Y. and J. W. Su, "Bandwidth enhancement of a printed wide-slot antenna with a rotated slot," *IEEE Transactions on Antennas and Propagation*, Vol. 53, 2111–2114, 2005.
16. Rani, R. B. and S. K. Pandey, "A parasitic hexagonal patch antenna surrounded by same shaped slot for WLAN, UWB applications with notch at vanet frequency band," *Microwave and Optical Technology Letters*, Vol. 58, 2996–3000, 2016.
17. Sung, Y., "Bandwidth enhancement of a microstrip line-fed printed wide-slot antenna with a parasitic center patch," *IEEE Transactions on Antennas and Propagation*, Vol. 60, 1712–1716, 2012.